Road Surface Roughness Estimation Using Polarimetric SAR Data

Arun Babu
Microwaves and Radar Institute
German Aerospace Center (DLR)
Wessling, Germany
arun.babu@dlr.de

Stefan V. Baumgartner
Microwaves and Radar Institute
German Aerospace Center (DLR)
Wessling, Germany
stefan.baumgartner@dlr.de

***Abstract*— The road surface roughness directly influences the grip and skid resistance of the vehicles. Since these parameters are relevant for the safety of the road users, they have to be continuously monitored to keep track of its changes. The potential of airborne polarimetric SAR to remotely monitor the road surface roughness is investigated in this study using fully polarimetric X-band data acquired with DLR's airborne radar sensor F-SAR. The polarimetric analysis revealed that the anisotropy and coherency matrix (T3) elements are sensitive to the road surface roughness. Additionally SAR backscatter based empirical models for surface roughness estimation were investigated.**

Keywords*— *F-SAR, Polarimetry, Sigma nought, Road surface roughness, Dubois model, Oh model

I. Introduction

The road infrastructure plays a major role in the economic growth of a country and issues with traffic infrastructure affect a nation's progress. Moreover, the condition of the road infrastructure has a major influence on safety, health and driving comfort [1]. The road surface roughness is one of the important parameters which affects the 'grip' or 'skid resistance' of the vehicle. A sufficient amount of skid resistance is required for performing safe acceleration, deceleration and steering maneuvers. Several studies have proven that poor skid resistance leads to a higher accident probability [2]. So, the road surface roughness needs to be continuously monitored to keep track of its present condition and changes.

In Germany, the road surface roughness is measured manually using measurement vehicles. But, this requires enormous costs for the entire road network because of its labor-intensive and time-consuming nature [3]. This study focuses on evaluating the potential of SAR to remotely estimate the road surface conditions on a large scale. So far, not much literature for road surface roughness estimation is available. The prime objective of this study is to investigate and develop efficient and reliable methods for road surface roughness estimation.

II. METHODOLOGY

A. SAR polarimetry based approach

The Polarimetric Synthetic Aperture Radar (PolSAR) is an advanced imaging radar system that uses the different polarization states of an Electromagnetic (EM) wave with the same center frequency to analyze the scattering information from different ground targets on the Earth's surface [4].

The polarimetric information obtained as 4 channels can be represented in the form of the Pauli basis vector (k_p) as follows [5]:

$$k_p = \frac{1}{\sqrt{2}}\begin{pmatrix} S_{HH} + S_{VV} \\ S_{HH} - S_{VV} \\ 2S_{HV} \end{pmatrix}. \quad (1)$$

By multiplying the Pauli basis vector with the transpose of its complex conjugate, the 3x3 coherency matrix $T3 = k_p \cdot k_p^{*T}$ can be obtained [6], [7]. The coherency matrix $T3$ can be used to derive the polarimetric parameters sensitive to the Root Mean Square (RMS) height (h_{rms}) which is widely used for the vertical roughness characterization (2):

$$h_{rms} = \sqrt{\frac{\sum_{i=1}^{n}\left(h_i - \bar{h}\right)^2}{n-1}} \quad (2)$$

where h_i is the vertical height at location i and $\bar{h}$ represents the mean vertical height of the surface for n samples [8], [9].

From the PolSAR data, the remotely sensed parameter (ks) can be derived which represents the effective vertical roughness. In this study, the polarimetric scattering anisotropy generated from the eigenvalues of the coherency matrix $T3$ and the elements of the $T3$ matrix itself is considered to generate the ks parameter.

According to the eigendecomposition theorem, the 3x3 coherency matrix $T3$ can be represented as follows [10]:

$$T3 = [U_3][\Sigma_3][U_3]^{-1}. \quad (3)$$

The 3x3 real, diagonal matrix $[\Sigma_3]$ contains the eigenvalues of $T3$ [11]:

$$[\Sigma_3] = \begin{bmatrix} \lambda_1 & 0 & 0 \\ 0 & \lambda_2 & 0 \\ 0 & 0 & \lambda_3 \end{bmatrix} \quad (4)$$

where $\infty > \lambda_1 > \lambda_2 > \lambda_3 > 0$.

The anisotropy parameter (A) is generated as follows [6], [11], [12]:

$$A = \frac{\lambda_2 - \lambda_3}{\lambda_2 + \lambda_3}. \quad (5)$$

The effective vertical roughness ks can be estimated from anisotropy as follows [8], [9]:

$$ks = 1 - A. \quad (6)$$

So, the ks estimated using the anisotropy parameter is based on the 2nd and 3rd eigenvalues of the coherency matrix.

The ks can also be estimated from the T_{22} and T_{33} elements of the coherency matrix as follows [6], [9]:

$$ks = 1 - \frac{T_{22} - T_{33}}{T_{22} + T_{33}}. \quad (7)$$

B. Empirical backscatter model-based approach

The Oh models developed in 1992 [13], 2004 [14] and the Dubois model developed in 1995 [15] for surface roughness and soil moisture estimation are considered here. These models were originally developed for bare soil and agricultural fields. The usability of these models for the surface roughness estimation of an asphalt road is evaluated in this study.

The inversion of the Oh model 1992 is based on solving the following non-linear equation using a root solving algorithm:

$$\left(\frac{2\theta}{\pi}\right)^{\frac{1}{\Gamma^o}} \left[1 - \frac{q}{0.23\sqrt{\Gamma^o}}\right] + \sqrt{p} - 1 = 0. \quad (8)$$

The above non-linear equation needs to be solved iteratively to estimate the Fresnel reflectivity of the surface at nadir (Γ^o). The parameter θ is the incidence angle, p is the co-polarized ratio and q is the cross-polarized ratio. The ks can be estimated from the Γ^o as follows:

$$ks = \ln\left(\frac{(\sqrt{p} + 1)}{\left(\frac{2\theta}{\pi}\right)^{\frac{1}{3\Gamma^o}}}\right). \quad (9)$$

The inversion of ks using the Dubois model is a two-step non-iterative process. The 1st step is to estimate the dielectric constant (ε') as follows:

$$\varepsilon' = \frac{\left(\log10\left(\frac{(\sigma^o_{HH})^{0.7857}}{\sigma^o_{VV}}\right) 10^{-0.19}\cos^{1.82}\theta \sin^{0.93}\theta\, \lambda^{0.15}\right)}{-0.024\tan\theta} \quad (10)$$

where σ^0_{HH} and σ^0_{VV} are the co-polar sigma nought values for HH and VV channels respectively. The 2nd step is to derive the ks from the estimated dielectric constant (ε') as follows:

$$ks = {\sigma^o_{HH}}^{1/1.4} 10^{2.75/1.4} \frac{\sin^{2.57}\theta}{\cos^{1.07}\theta} 10^{-0.02\varepsilon'\tan\theta} \lambda^{-0.5}. \quad (11)$$

In the Oh model 2004, the surface moisture (mv) is estimated to derive the ks in contrast to the Oh model 1992. The surface moisture (mv) is estimated by solving the following non-linear equation using an iterative root-finding algorithm:

$$1 - \left(\frac{\theta}{90}\right)^{0.35mv^{-0.65}} e^{-0.65} \left[\left[-3.125\ln\left\{1 - \frac{\sigma^o_{VH}}{0.11mv^{0.7}\cos^{2.2}\theta}\right\}\right]^{0.556}\right]^{1.4} - p = 0. \quad (12)$$

Then the ks is estimated as follows:

$$ks = \left[-3.125\ln\left\{1 - \frac{\sigma^o_{VH}}{0.11mv^{0.7}\cos^{2.2}\theta}\right\}\right]^{0.556}. \quad (13)$$

The Root Mean Square (RMS) height (h_{rms}) can be derived from the ks using the following equation:

$$h_{rms} = \frac{ks}{(2\pi/\lambda_c)} \quad (14)$$

where λ_c is the center frequency of the SAR system.

The ks values estimated from the Oh models have a validity range of $0.1 < ks < 6.0$ [13], [14]. This corresponds to a h_{rms} validity range of 0.49 mm < h_{rms} < 29.82 mm for a X-band sensor with 9.60 GHz frequency. For the Dubois model, the measured ks values are valid when ks < 2.5 and the incidence angle (θ) >30° [15]. This corresponds to a h_{rms} validity range of h_{rms} < 12.43 mm for a X-band sensor with 9.60 GHz frequency.

III. STUDY AREA AND DATASETS

The first study area is the Kaufbeuren test site located in Bavaria, Germany, and the second study area is the test site near the motorway intersection Cologne-East, also Germany, where the "Bundesanstalt für Straßenwesen (BASt)" operates the duraBASt test site.

The Kaufbeuren test site was a former military airfield and includes the runway, taxiways and parking areas composed of different materials (e.g., asphalt, concrete) and, thus, have a different surface roughness (Fig. 1).

Fig. 1. Kaufbeuren test site showing zoomed view of the cracked parking area

The duraBASt test site contains road surfaces made of different materials (asphalt, concrete, etc.) having also different roughness.

Fig. 2. Cologne motorway intersection showing zoomed view of two duraBASt test sites

The X-band quad-pol data acquired with DLR's airborne F-SAR sensor over these two test sites are used for this study.

IV. PRELIMINARY RESULTS

This study was started in September 2019 and the initial results of the road surface roughness using the techniques described in the previous section are discussed here.

Fig. 3 shows the intensity HH image of the Kaufbeuren test site. The runway and the cracked parking area are indicated in the image.

Fig. 4 shows the intensity HH image of the Cologne motorway intersection. One of the duraBASt test sites shown at the right top position in Fig. 2 is indicated in Fig. 4.

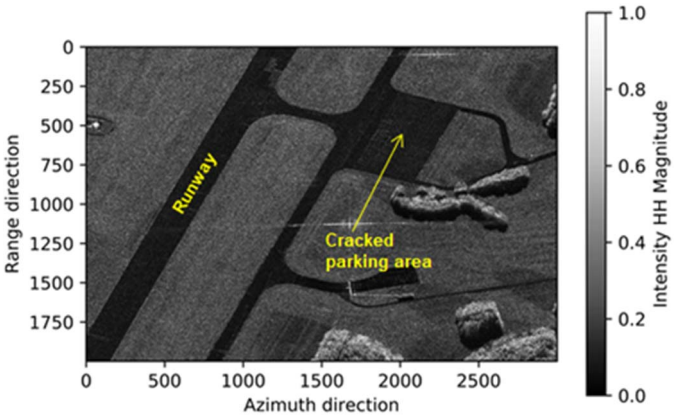

Fig. 3. Intensity HH image of the Kaufbeuren test site

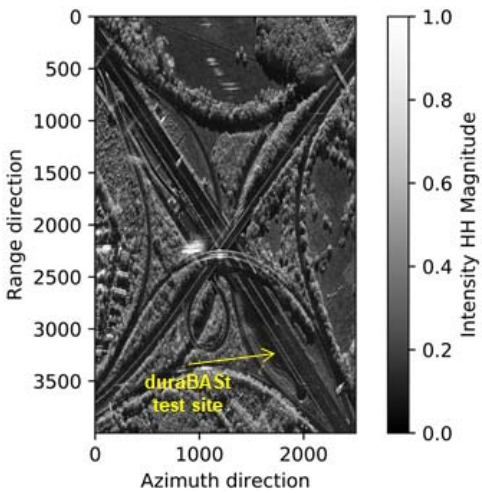

Fig. 4. Intensity HH image of the duraBASt test site

Fig. 5 (a) shows the h_{rms} image of the cracked road area shown in Fig. 1 and its surrounding grasslands estimated from the anisotropy parameter. The cracked road areas and the grasslands are showing similar values of h_{rms} and the smooth road sections are showing comparatively lower values of h_{rms} . The cracked road area shown by the red circle in Fig. 5 (a) is having a mean h_{rms} value of 2.89 mm and the smooth road area shown by the yellow circle is having a mean h_{rms} value of 2.15 mm.

Fig. 5 (b) shows the h_{rms} image generated from the $T3$ matrix elements. A similar trend in roughness variation can be observed in both figures. But, Fig. 5 (b) shows higher values of roughness for the same areas in Fig. 5 (a). The cracked road area shown by the red circle is having a mean h_{rms} of 3.83 mm and the comparatively smooth road area shown by the yellow circle is having a mean h_{rms} value of 2.57 mm. The roads and surrounding grasslands can be better differentiated in Fig. 5 (b) compared to Fig. 5 (a).

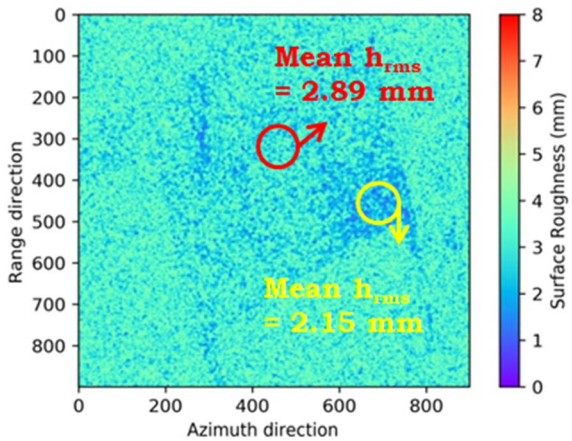

(a)

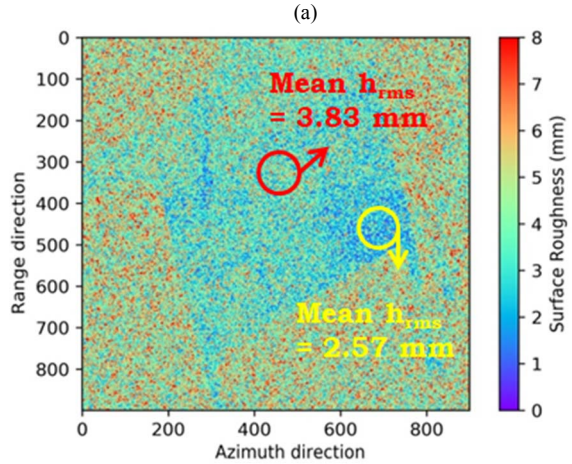

(b)

Fig. 5. h_{rms} images; (a) from Anisotropy; (b) from the T3 matrix.

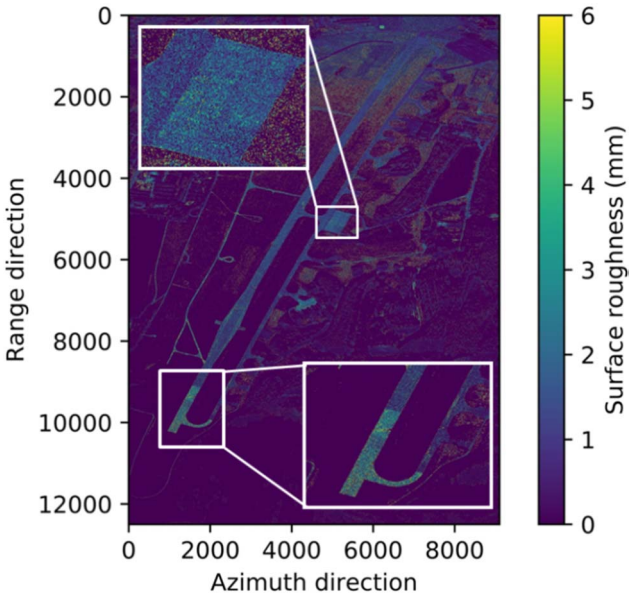

Fig. 6. h_{rms} image of Kaufbeuren test site generated using Dubois model

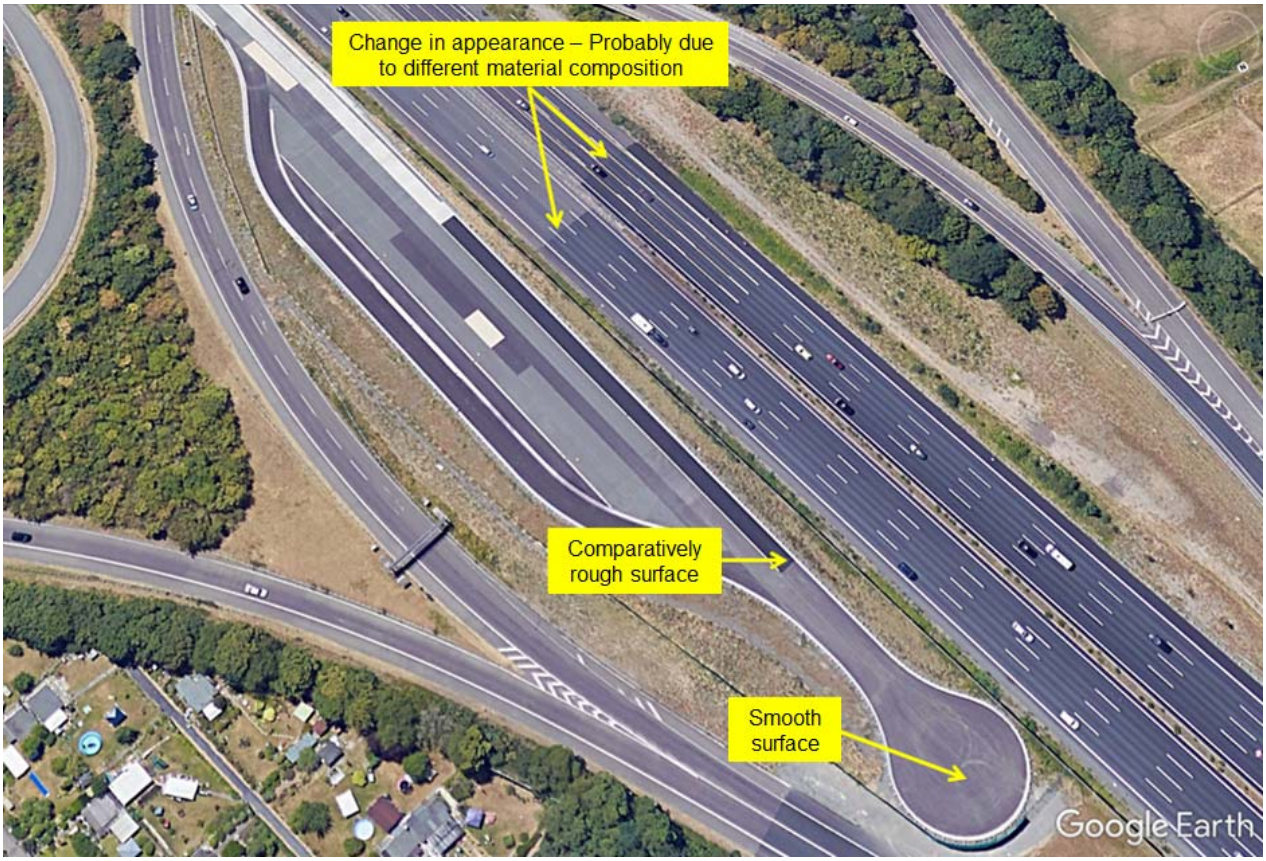

(a)

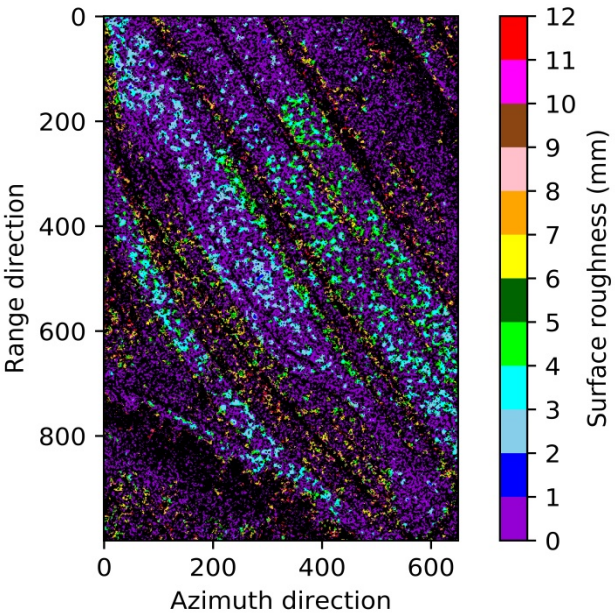

(b)

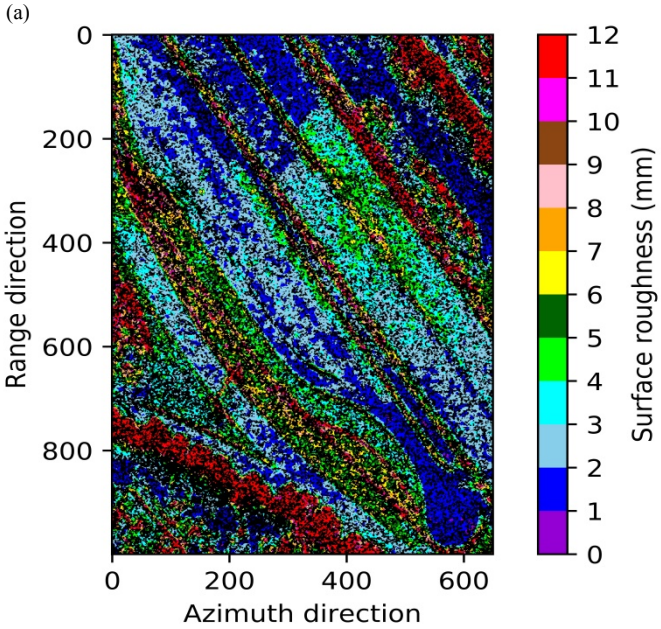

(c)

Fig. 7. duraBASt test site images; (a) Google Earth image; (b) h_{rms} image generated using Oh 2004 model; (c) h_{rms} image generated using Dubois model

Fig. 6 shows the h_{rms} image of the entire Kaufbeuren test site generated using the empirical Dubois model. The zoomed view on the left top side of the image shows the cracked road area shown in Fig. 5. Here also a higher value of h_{rms} can be observed at the more cracked locations. The zoomed view on the right bottom of the image shows the region of the runway with different road materials (asphalt and concrete). So, the difference in the h_{rms} between different road materials can be clearly identified here. But, this difference in h_{rms} can also be probably due to the change in the dielectric constant of the two road materials which needs to be further investigated.

Fig. 7 (a) shows the Google Earth view of the duraBASt test site and the AutoBahn. The smooth regions and comparatively rough regions of the duraBASt test site are indicated in Fig. 7 (a). A change in appearance of the Autobahn road surface can be seen in the Google Earth image which may be due to the different material composition which is also highlighted in Fig. 7 (a).

Fig. 7 (b) shows the h_{rms} image generated using the empirical Oh 2004 model. By comparing Fig. 7 (b) with Fig. 7 (a) it can be seen that the smooth region highlighted in Fig. 7 (a) is having lower values of h_{rms} in the 0-1 mm range appearing in purple colour. The comparatively rough regions shown in Fig. 7 (a) can be found to be showing higher values of surface roughness in the 4-5 mm range appearing in green colour (Fig. 7 (b)). It can also be found that the highlighted portions of the autobahn are also showing a change in roughness values in Fig. 7 (b).

The h_{rms} image generated using the Dubois model is shown in Fig. 7 (c). By comparing Fig. 7(c) with Fig. 7 (b) it can be seen that the change in surface roughness at the highlighted regions in Fig. 7 (a) can be better distingushed in Fig. 7 (c). But the smooth regions are showing comparatively higher values of surface roughness in Fig. 7 (c) compared to Fig. 7 (b). But these results needs to be further analysed with respect to the ground truth to validate the absolute surface roughness values.

V. CONCLUSION

Polarimetric data are sensitive to road surface roughness and thus show great potential for wide-area road surface condition monitoring. The anisotropy and $T3$ matrix elements are showing a variation in (h_{rms}) between smooth and cracked road regions. The empirical models developed for the surface roughness and soil moisture estimation of bare soils and agricultural lands have the potential to estimate the millimeter level surface roughness of smooth road surfaces. Compared to the SAR polarimetry-based approach, the SAR backscatter based empirical models are less affected by noise and provides a better differentiation between the road and surrounding regions. The Dubois model is showing better discrimination between the smooth and rough road regions compared to the other models. But, all the results estimated using the different models need to be validated with respect to the ground truth data. Because so far, although the models provided the surface roughness results with mm as unity, it is not clear whether these estimated "absolute/average roughness" values really represent the true surface roughness and this investigation is currently in progress. Also, futher experiments are planned using a Ka-band sensor which, due to the smaller wavelength, will be much more sensitive to the roughness differences and suitable for detecting smaller cracks and potholes.

REFERENCES

[1] J. Hofmockel, J. Masino, J. Thumm, E. Sax, and F. Gauterin, "Multiple vehicle fusion for a robust road condition estimation based on vehicle sensors and data mining," *Cogent Eng.*, vol. 5, no. 1, pp. 1–15, 2018.

[2] H. Liu, Z. Zhang, D. Guo, L. Peng, Z. Bao, and W. Han, "Research progress on characteristic technique of pavement micro-texture and testing technology of pavement skid resistance at home and abroad," in *2011 International Conference on Remote Sensing, Environment and Transportation Engineering*, 2011, pp. 4368–4372.

[3] K. Laubis, "Crowd-Based Road Surface Monitoring and its Implications on Road Users and Road Authorities," Karlsruhe Institute of Technology, Germany, 2017.

[4] C. Si-wei, X. Wang, S.-P. Xiao, and Sato M, *Target Scattering Mechanism in Polarimetric Synthetic Aperture Radar Interpretation and Application*. Singapore: Springer Nature, 2018.

[5] I. H. Woodhouse, *Introduction to microwave remote sensing*. New Delhi, India: CRC Press, Taylor & Fancis Group, 2009.

[6] I. Hajnsek, "Inversion of Surface Parameters Using Polarimetric SAR," Friedrich Schiller University Jena, 2001.

[7] J. Van Zyl and Y. Kim, *Synthetic Aperture Radar Polarimetry*, 1st edition. New Jersey: Wiley-Blackwell, 2011.

[8] P. Marzahn and R. Ludwig, "On the derivation of soil surface roughness from multi parametric PolSAR data and its potential for hydrological modeling," *Hydrol. Earth Syst. Sci.*, pp. 381–394, 2009.

[9] T. Jagdhuber, "Soil Parameter Retrieval under Vegetation Cover Using SAR Polarimetry," University of Potsdam, 2012.

[10] C. M. H. Unal and L. P. Ligthart, "Decomposition Theorems applied to Random and Stationary Radar Targets," *Prog. Electromagn. Res.*, pp. 45–66, 1998.

[11] E. Pottier, J.-S. Lee, and L. Ferro-Famil, "Advanced Concepts in Polarimetry – Part 1," vol. 2, no. October, pp. 21–22, 2004.

[12] J. A. Richards, *Remote Sensing with Imaging Radar*. Springer International Publishing, 2009.

[13] Y. Oh, K. Sarabandi, and F. T. Ulaby, "An empirical model and an inversion technique for radar scattering from bare soil surfaces," *IEEE Trans. Geosci. Remote Sens.*, vol. 30, no. 2, pp. 370–381, Mar. 1992.

[14] Yisok Oh, "Quantitative retrieval of soil moisture content and surface roughness from multipolarized radar observations of bare soil surfaces," *IEEE Trans. Geosci. Remote Sens.*, vol. 42, no. 3, pp. 596–601, Mar. 2004.

[15] P. C. Dubois, J. van Zyl, and T. Engman, "Measuring soil moisture with imaging radars," *IEEE Trans. Geosci. Remote Sens.*, vol. 33, no. 4, pp. 915–926, Jul. 1995.